Crystal structure of the sodium-potassium pump (Na^+,K^+-ATPase) with bound potassium and ouabain

Haruo Ogawa[a], Takehiro Shinoda[a,1], Flemming Cornelius[b], and Chikashi Toyoshima[a,2]

[a]Institute of Molecular and Cellular Biosciences, The University of Tokyo, Bunkyo-ku, Tokyo 113-0032, Japan and [b]Department of Physiology and Biophysics, University of Aarhus, DK-8000 Aarhus C, Denmark

Contributed by Chikashi Toyoshima, June 24, 2009 (sent for review June 11, 2009)

The sodium-potassium pump (Na^+,K^+-ATPase) is responsible for establishing Na^+ and K^+ concentration gradients across the plasma membrane and therefore plays an essential role in, for instance, generating action potentials. Cardiac glycosides, prescribed for congestive heart failure for more than 2 centuries, are efficient inhibitors of this ATPase. Here we describe a crystal structure of Na^+,K^+-ATPase with bound ouabain, a representative cardiac glycoside, at 2.8 Å resolution in a state analogous to E2·2K^+·Pi. Ouabain is deeply inserted into the transmembrane domain with the lactone ring very close to the bound K^+, in marked contrast to previous models. Due to antagonism between ouabain and K^+, the structure represents a low-affinity ouabain-bound state. Yet, most of the mutagenesis data obtained with the high-affinity state are readily explained by the present crystal structure, indicating that the binding site for ouabain is essentially the same. According to a homology model for the high affinity state, it is a closure of the binding cavity that confers a high affinity.

cardiac glycosides | crystallography

Ouabain, derived from a plant *Strophanthus gratus*, represents a class of cardiac glycosides, or digitalis-like compounds, that have been used in the treatment of congestive heart failure and supraventricular arrhythmias for >200 years. They inhibit the activity of Na^+,K^+-ATPase and thereby increase the intracellular Na^+ concentration, which in turn slows down a Na^+/Ca^{2+} exchanger resulting in an increase in intracellular Ca^{2+} concentration and stronger muscle contraction (see ref. 1 for a recent review). However, their therapeutic index is low, and structural information on their binding has been keenly sought. Many mutagenesis (2–9) and modeling studies have been carried out, and an enormous body of literature has accrued on the structure-activity relationships of various cardiac glycosides (10–12). However, how ouabain binds to the ATPase is still elusive. In particular, it binds to the ATPase in various states in the reaction cycle with different affinities. Although it is established that it binds with high affinity to the ATPase in E2P-like states [$K_d \approx 0.7$ nM for shark enzyme used here (13)], the ATPase-ouabain complexes formed by the forward (i.e., in the presence of ATP + Na^+ + Mg^{2+}) and backward (i.e., in the presence of Pi + Mg^{2+}) reactions have different properties (14). Particularly complicated is the effect of K^+, which accelerates the dephosphorylation of the ATPase and thereby antagonizes ouabain binding. Yet, ouabain binds to the ATPase even in the E2·2K^+ state, although at a mM affinity, and stabilizes the occlusion of K^+ (15). Thus, the binding in this state is specific (14, 15), although the affinity is low. Clinically, the antagonism between cardiac glycosides and serum K^+ is a well-known factor in cardiac glycoside toxicity. Therefore, the low affinity structure in a K^+-bound state is also important, because it may shed light on the mechanism of the antagonism.

Here we describe a 2.8 Å resolution crystal structure of the Na^+,K^+-ATPase in a state analogous to E2·2K^+·Pi with bound ouabain and compare it to the unbound form (16) and the corresponding form of Ca^{2+}-ATPase (17). As K^+ ions are found in the transmembrane binding sites, the structure is considered to represent a low-affinity ouabain-bound state (14, 15). Ouabain is wedged very deeply between transmembrane helices, partly unwinding the M4 helix. Thus, the crystal structure supports the proposal that the M5 and M6 helices are the main binding site (2, 9), but urges reconsideration of previous studies that have placed ouabain on the extracellular surface of the ATPase α-subunit.

Results and Discussion

Identification of the Ouabain Binding Site. Crystals of Na^+,K^+-ATPase from shark rectal gland were generated by fixing the ATPase in a state analogous to E2·2K^+·Pi with a stable phosphate analog MgF_4^{2-} (16). The crystals were soaked in a buffer containing 20 mM ouabain for 5 h. The structure was solved by molecular replacement starting from the ouabain-unbound form (16) and refined to an R_{free} of 29.3% at 2.8 Å resolution (Table 1).

As a whole, structural changes caused by ouabain binding are rather small, limited to transmembrane helices M1–M4 (Figs. 1*A* and 2 *A* and *B*). If the ouabain-unbound structure is aligned to the bound one with the transmembrane region, the cytoplasmic headpiece appears slightly inclined toward the M5–M1 direction (i.e., around the y-axis), reflecting a small change of the M5 helix. The largest difference is observed with the extracellular half of the M4 helix (M4E), which moves away from M6 (Fig. 2*B*). M1–M2 helices move into the space created by the movement of M4. As a result, in this ouabain-bound form, the cavity surrounded by M1–M2 and M4E–M6 is larger and opened to the extracellular medium (Figs. 2*B* and 3).

The difference Fourier (F_{obs} - F_{calc}) electron density map before including ouabain in the atomic model (Fig. S1) unambiguously located the bound ouabain in this cleft. At a contour level of 5σ, there was only 1 positive density that could be assigned to ouabain in the density map; at 4σ the density showed a characteristic chair shape of a steroid system. An omit-annealed difference map (Fig. 1*B*) was of a good quality, nicely defining the position and the orientation of ouabain. Contrary to previous models that placed ouabain on the extracellular surface, it is deeply inserted into the transmembrane cleft (Fig. 1*A*). Yet, the locations of >30 residues influencing ouabain binding as identified by mutagenesis studies (2–9), (small spheres in Fig. S1) nicely delineate the binding site, although with some exceptions (e.g., those on M7–M10). As all of the mutagenesis studies have been carried out with high-affinity ouabain-bound states, the critical residues do not necessarily coincide with the ouabain binding residues in the crystal structure of a low affinity state.

Author contributions: F.C. and C.T. designed research; H.O., T.S., F.C., and C.T. performed research; H.O. and C.T. analyzed data; and F.C. and C.T. wrote the paper.

The authors declare no conflict of interest.

Data deposition: The atomic coordinates have been deposited in the Protein Data Bank, www.pdb.org (PDB ID 3A3Y).

[1]Present address: Systems and Structural Biology Center, RIKEN, Tsurumi-ku, Yokohama, 230-0045, Japan.

[2]To whom correspondence should be addressed: E-mail: ct@iam.u-tokyo.ac.jp.

This article contains supporting information online at www.pnas.org/cgi/content/full/0907054106/DCSupplemental.

Table 1. Data collection and refinement statistics

Data collection	
Space group	*C*2
No. crystals	2
Cell dimensions	
a, *b*, *c* (Å)	222.9, 50.7, 163.3
β (°)	104.6
Resolution (Å)	50.0–2.8 (2.9–2.8)*
R_{merge}	4.5 (38.8)
I/σ_I	30.3 (3.2)
Completeness (%)	99.9 (100.0)
Redundancy	10.4 (8.2)
Refinement	
Resolution (Å)	15–2.8 (2.87–2.80)
No. reflections	42,690 (3,052)
R_{work}/R_{free}	0.247/0.293 (0.338/0.421)
No. atoms	10,308
Protein	10,122
Ligand/ion	120
Water	66
B-factors	
Protein	62.9
Ligand/ion	94.8
Water	37.7
R.m.s deviations	
Bond lengths (Å)	0.007
Bond angles (°)	1.210

*Highest resolution shell is shown in parenthesis.

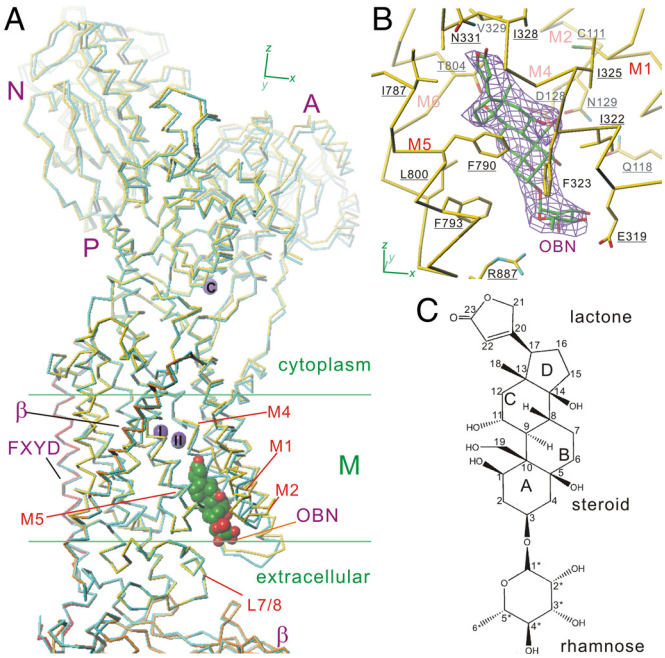

Fig. 1. Crystal structure of Na^+,K^+-ATPase with bound ouabain. (*A*) Superimposition of Cα traces of Na^+,K^+-ATPase from shark rectal gland in ouabain-bound (yellow) and ouabain-unbound (cyan) forms, viewed along the membrane plane. Na^+,K^+-ATPase is fixed in a state analogous to E2·2K^+·Pi, with MgF_4^{2-} as a stable phosphate analog. Ouabain (OBN; green and red) and K^+ ions (I, II, and c; purple) are shown in space fill. The β-subunit, FXYD protein, 3 cytoplasmic domains (A, N, and P), and several transmembrane helices are marked. Green horizontal lines indicate the approximate position of lipid bilayer (M). (*B*) An F_{obs} - F_{calc} omit-annealed map of ouabain at 3σ, superimposed on the final atomic model. The underscores indicate that the residues have been identified as affecting ouabain binding by mutagenesis. (*C*) A diagram of ouabain.

The strong coincidence here indicates that the binding site itself is essentially the same in the low and high affinity states.

Binding of the Lactone Ring. Cardiac glycosides have a tripartite structure: A 5- or 6-membered lactone ring, a steroid core and a carbohydrate moiety consisting of 1–4 residues (Fig. 1*C*). Ouabain has a 5-membered lactone and rhamnose as the carbohydrate. Each part appears to have a different role in binding. As summarized by Glynn (18), critical features of cardiac glycosides are: (*i*) The unsaturated lactone ring attached in the correct configuration at C17; (*ii*) the *cis* configuration of the AB and CD ring junctions in the steroid nucleus; (*iii*) the presence of a hydroxyl group at C14; and (*iv*) the presence of an appropriate sugar at C3. The crystal structure explains why.

The lactone ring is located very close to Val-329 and Ala-330 in the M4E helix (Fig. 4 and Fig. S2), pushing Gly-326 away (Fig. 2*A*), so that the original hydrogen bonds of the carbonyl with Val-329 and Ala-330 amides are broken and substituted by hydrogen bonds with the carbonyl conjugated to the lactone ring (Fig. 4 and Fig. S2). As a result, the distance between Gly-326 and Thr-804 is ≈5 Å wider, and the M4E helix unwound by 1 more turn (now between Gly-326 and Gly-335; Fig. 2*A*). The carbonyl of Ile-327 appears stabilized now by the Asn-331 side chain (Fig. S2). The coordination of K^+ is partially destroyed, because Val-329, which provides the carbonyl oxygen to site II K^+ (16), is displaced. Yet, we still see strong electron density peaks that represent bound K^+ ions, suggesting that the proximity of lactone to site II K^+ is the reason why dissociation of bound K^+ is blocked by ouabain (14, 15).

Thus, the position of the carbonyl group conjugated to the unsaturated lactone ring (Fig. 1*C*) must be critically important. Indeed there is a strong correlation between the potency of a glycoside and the position of the carbonyl group (10), and saturation of the lactone ring causes a most dramatic (nearly 2 orders of magnitude) reduction in affinity (12), due to change in its orientation relative to the steroid core. Around the lactone ring the geometry is very tight (i.e., strong van der Waals contacts; Fig. 4*A*). That is why addition of any side chain to Gly-326 causes a large reduction of ouabain affinity (9). Without bound K^+, unwinding of the M4 helix and, therefore, the accommodation of the lactone ring, would be much easier. In fact, addition of K^+ dissociates ouabain if the concentration of ouabain is less than saturating (19). Thus, stabilization of the helix conformation by K^+ will at least partly explain the low affinity of ouabain in the presence of K^+.

Binding of the Steroid Core. The steroid core is tightly held in a cavity lined by M4–M6 helices. Three Phe residues (Phe-323 on M4, Phe-790 and Phe-793 on M5; Figs. 3*B* and 4*A*) form a complementary surface to the α-side of the steroid core, dictating a *cis* configuration of the AB and CD ring junctions. The side chain of Phe-790 stacks with the steroid core. In the ouabain-unbound form, these 3 Phe and 2 Leu/Ile (Ile-322 on M4 and Leu-800 on M6) form a hydrophobic cluster, leaving no space at all for this part of ouabain (Figs. 3*A* and 4*B*). The side chains of Phe-323 and Phe-790 flip to accommodate the steroid core (Fig. S2). All of these hydrophobic residues, except for Phe-323, have been identified as critical by mutagenesis studies (6, 8). Even changing 1 of these Phe to Tyr would either prevent this rearrangement or directly interfere with ouabain binding, explaining mutational results (8). The binding cavity is thus created primarily by movement of M4E (Fig. 2). The other side (β-side) of the steroid core faces the cavity with little interactions with protein residues (Figs. 3*B* and 6), presumably the main reason for the low affinity of ouabain in this state.

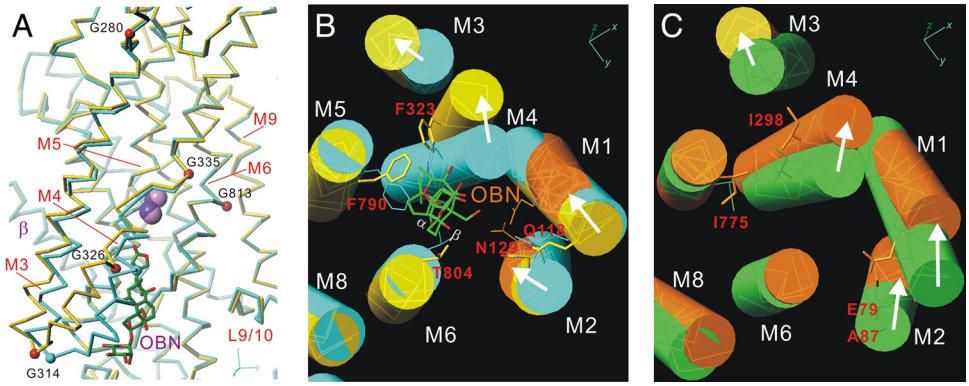

Fig. 2. Structural changes in the transmembrane region of Na^+,K^+-ATPase due to ouabain binding and corresponding changes in Ca^{2+}-ATPase. (*A*) Superimposition of Cα traces of Na^+,K^+-ATPase in ouabain-bound (yellow) and ouabain-unbound (cyan) forms, viewed parallel to the membrane plane in approximately orthogonal direction to Fig. 1*A*. Ouabain (OBN; green and red) is shown in stick, and K^+ ions (I and II; purple) are shown in space fill. Locations of Gly residues involved in structural changes are marked with small balls. M1 and M2 helices are cut away for clarity. (*B* and *C*) Superimposition of transmembrane helices (cylinders) viewed approximately perpendicular to the membrane plane from the extracellular side. (*B*) Na^+,K^+-ATPase in the state analogous to E2·2K^+·Pi (cyan) and that with bound ouabain at low affinity (yellow) and a hypothetical one for high-affinity ouabain-bound state (E2P, orange). (*C*) Ca^{2+}-ATPase in the states analogous to the E2·Pi product state (green; PDB ID, 1WPG) and the E2P ground state (orange; PDB ID, 2ZBE). Arrows show the movements of transmembrane helices accompanying the E2·Pi → E2P transition.

The hydroxyl group at C14β, on the junction between the C and D rings, forms a hydrogen bond with Thr-804 (Fig. 4*A* and Fig. S2*A*), a very critical residue in ouabain binding (5, 8). Thus, a role of the hydroxyl at C14 is now clarified. In contrast, the hydroxyl at C11α is not bonded, and in fact, digitoxin (with no hydroxyl group at C11 or C12) has a 4 times higher affinity than digoxin (with a sterically unfavorable hydroxyl at C12) (12). Some space is available around C16, allowing an addition of the acetyl group without large impact on the affinity (12).

Binding of the Sugar Moiety. The rhamnose residue can make hydrogen bonds with Arg-887 in the L7/8 loop and Glu-319 on M4 (Fig. 3*B* and Fig. S2*A*), thereby conferring a much higher [≈300 times (12)] affinity to ouabain than ouabagenin, which lacks the sugar moiety. Photoaffinity functional groups inserted between 2* and 3* of rhamnose form cross-links with the N-terminal 41-K fragment of the ATPase (20), consistent with the orientation of the sugar residue here. Deleterious effect of a substitution of the methyl group at 6* with hydroxyl (21) is readily explained by the hydrophobic environment of this group (Figs. 3*B* and 4*A*). The vacant space around the sugar residue is quite large (Fig. 4*A*), and filling that space may enhance the affinity [e.g., addition of anthracene increases the affinity 2-fold (12)]. An antibody against the loop connecting the M1 and M2 helices is known to enhance the affinity of ouabain (22). Because the interactions with the sugar moiety have such a large effect on the affinity, it is conceivable that the β-subunit of the ATPase changes ouabain affinity (23) by altering the positions of interacting residues [e.g., Arg-887, a mutation sensitive residue (4)] on the L7/8 loop, the primary interface with the β-subunit.

Creation of the Binding Cavity. For ouabain to be able to bind to the ATPase in the E2·2K^+·Pi state, the binding cavity had to be formed through rearrangement of the M1–M4 helices (Fig. 2). As mentioned earlier, the largest movement was observed with M4E. Here the segment between 2 Gly residues, that is, Gly-335 in the conserved PEGL motif just above the K^+-binding site and

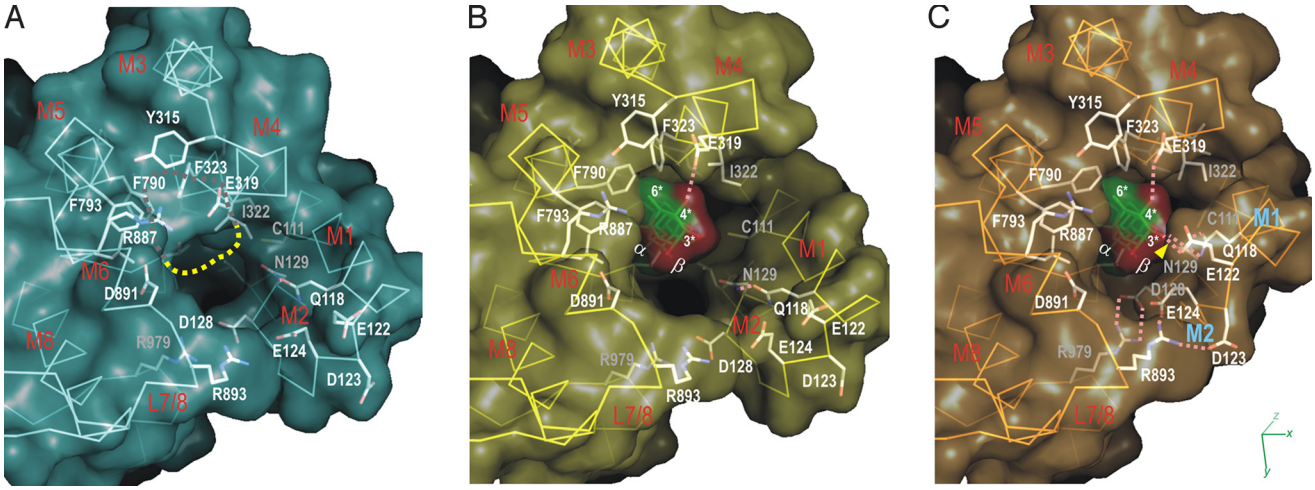

Fig. 3. Binding of ouabain to the transmembrane binding site, viewed approximately perpendicular to the membrane plane from the extracellular side. Water accessible surface superimposed on the atomic model. (*A*) Ouabain-unbound state. (*B*) Low-affinity ouabain-bound state. (*C*) Hypothetical one for high-affinity ouabain-bound state. Dotted orange lines show likely hydrogen bonds. Dotted yellow line in panel *A* shows the outline of ouabain placed at the same position in panel *B*. The α- and β-sides and van der Waals surface of ouabain (green and red) are shown in panels *B* and *C*.

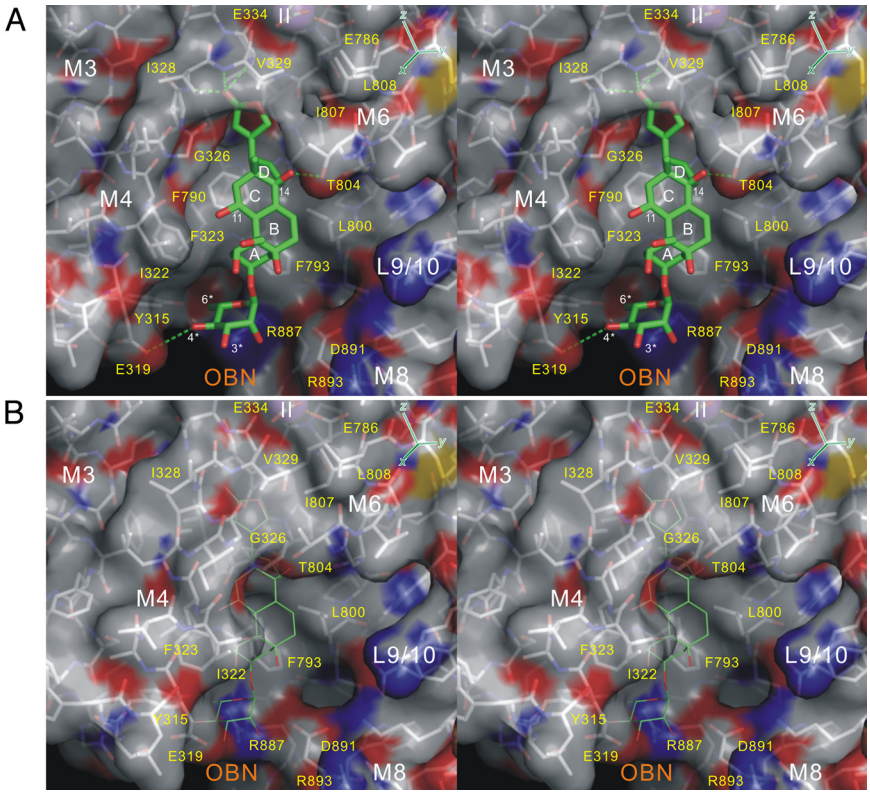

Fig. 4. Structural changes around the M4–M6 transmembrane helices on ouabain binding. Viewed in stereo approximately parallel to the membrane. Water accessible surface in atom color (*A*, ouabain-bound with low affinity; *B*, ouabain-unbound) superimposed with the respective atomic models. Ouabain (OBN; green and red sticks) in panel *B* is placed at the same position as in panel *A*. Green dotted lines show likely hydrogen bonds.

Gly-314 in the loop connecting the M3 and M4 helices, inclines ≈15 ° away from M6 (Fig. 2). As a result, the space becomes ≈5 Å wider at the position of the A-ring of the steroid (Fig. 4). M3 moves in a direction ≈45 ° different from M4 (Fig. 2*B*), suggesting that it is pushed by M4E and a change in dihedral angle of Gly-314 determines the direction. These movements of transmembrane helices are very similar to those observed in the crystal structures of Ca^{2+}-ATPase between E2·MgF_4^{2-}(TG) and E2·BeF_3^- (24), that is, between an E2·Pi product state and an E2P ground state analogs (Fig. 2*C*). Indeed, Ca^{2+}-ATPase crystal structures also show cavities, although smaller, at equivalent positions to the one through which ouabain reaches the binding site in the E2·Pi analog and the one into which the steroid core fits in the E2P ground state analog (Fig. 5)

Another major difference between the E2·Pi and the E2P ground state analogs of Ca^{2+}-ATPase is the position of the V-shaped structure formed by the M1 and M2 helices (24), which is 1 turn of an α-helix shifted toward the cytoplasm in E2P (Fig. 2*C*). This movement is related to a rotation of the A-domain, and prohibited in the present crystal of Na^+,K^+-ATPase due to stabilization by crystal packing and bound K^+.

Homology Modeling of the High-Affinity Ouabain-Bound State. The similarity of the movement observed for the M3–M6 helices in the 2 ATPases prompted us to carry out homology modeling based on the E2·BeF_3^- (i.e., E2P) crystal structure of Ca^{2+}-ATPase (Fig. 2 *B* and *C*). In this high affinity model, in which ouabain is placed in the same way with respect to the M4–M6 helices, the M1 and M2 helices come much closer to ouabain forming a rather complementary surface, stabilized by several hydrogen bonds [Asp-128 (M2)-Arg-979 (L9/10), Asp-123/Glu-124 (L1/2)-Arg-893 (L7/8); Figs. 3*C* and 6]. The Glu-122 side chain located on the L1/2 loop now comes within a hydrogen bond distance from the hydroxyl group at C3* in rhamnose (the arrowhead in Fig. 3*C*), likely contributing to high affinity binding. This feature agrees well with the observation that the NH_2 substitution of the hydroxyl at C4* provides the highest affinity (25), because it will form a hydrogen bond with Glu-122 as well as Glu-319 (Fig. 3*C*), a residue affecting ouabain binding (8).

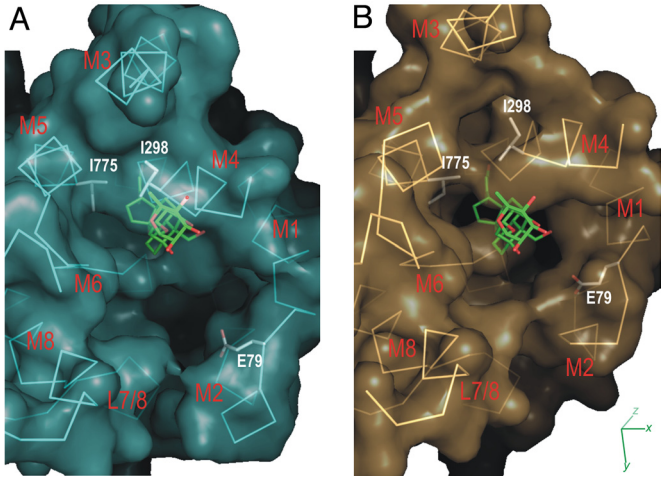

Fig. 5. Structural changes between the E2P ground state and the E2·Pi product state observed in the crystal structures of Ca^{2+}-ATPase. Viewed approximately perpendicular to the membrane plane from the extracellular side. Water accessible surface superimposed on the atomic model. (*A*) E2·Pi product state [E2·MgF_4^{2-}(TG); PDB ID: 1WPG]. (*B*) E2P ground state (E2·BeF_3^-; PDB ID: 2ZBE). Atomic models of ouabain are placed in the positions corresponding to that observed in the Na^+,K^+-ATPase crystal structure (Fig. 3*B*).

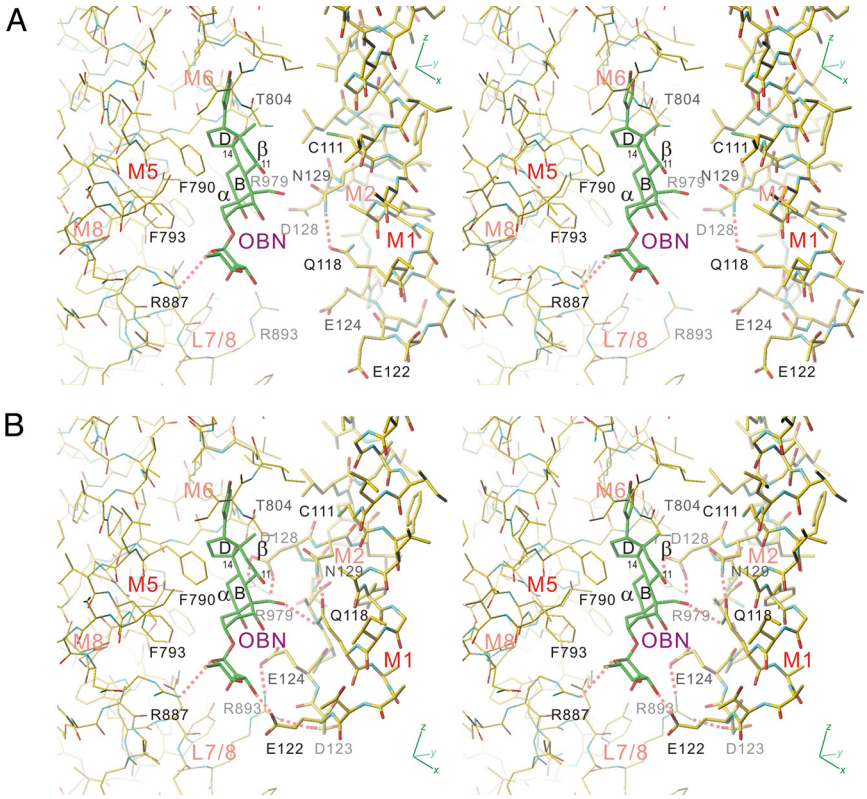

Fig. 6. Details of the ouabain binding site. (*A*) Crystal structure of the low-affinity ouabain (OBN)-bound state. (*B*) Hypothetical one for the high-affinity ouabain-bound state. Viewed in stereo approximately parallel to the membrane. The B and D rings and the α- and the β-sides of ouabain are identified. Orange dotted lines show likely hydrogen bonds.

There are 3 hydroxyl groups on the A- and B-rings of the steroid core of ouabain sticking out from the β-side toward the M1–M2 helices (Fig. 6). Gln-118 (M1) and Asn-129 (M2) have been recognized as critical residues, because their substitutions by Arg and Asp, respectively, as found in rodent α1, cause a large reduction in ouabain inhibition (2). These 2 residues form hydrogen bonds to maintain the V-shaped structure formed by the M1 and M2 helices. In the model for the high affinity state, the Gln-118 side chain comes close enough to the hydroxyl at C19 to form a hydrogen bond (Fig. 6). However, as Lingrel pointed out (2), it is unlikely to make a major contribution. In fact, even the Gln118Ala-Asn129Ala double mutant exhibits a high affinity for ouabain (3). On the contrary, double mutation of Gln118Asp-Asn129Arg is 40 times more effective than the Gln118Arg-Asn129Asp mutation in reducing the affinity (2). Having Arg at the inner position will cause a larger steric hindrance to closure of the cavity (Fig. 6). Furthermore, evomonoside, which has no hydroxyls other than the critical one at C14, has the highest affinity of 37 derivatives examined in reference (12). Asp-128 is unlikely to contribute directly to ouabain binding, yet its substitution by Asn causes a 60 times reduction in affinity (3). The high affinity model readily provides an explanation, as Asp-128 will form salt bridges with Arg-979 on closure of the cavity (Figs. 3*C* and 6*B*). Unfortunately no literature could be identified for mutations of other residues likely involved in the closure. At any rate, all of the quoted data suggest that having a more hydrophobic and flatter interface between cardiac glycosides and the M1–M2 helices increases the affinity, presumably by making a more complementary interface.

Thus, the high affinity of cardiac glycosides appears to be conferred, at least in part, by a complementary interface with Na^+,K^+-ATPase. In this regard, it is similar to thapsigargin, a very high affinity [K_d of pM range (26)] transmembrane inhibitor of Ca^{2+}-ATPase. It forms only 1 hydrogen bond with Ca^{2+}-ATPase (27), and the substitution of Phe (Phe-256) that forms a part of the complementary surface largely reduces its affinity (28). Similarity with the binding pockets of steroid receptors (29) is also evident. Thus, the reason for the low affinity for ouabain in the current E2·2K^+·Pi state is most likely that the closure of the binding cavity is blocked by bound K^+.

Conclusion

Although the present crystal structure represents a low affinity state, it very nicely explains many mutagenesis results (2–9) and structure-activity relationships of digitalis-like compounds (10–12) and leads us to a plausible model for a high affinity state. Obviously it has to be confirmed by the crystal structure of the high affinity state, but at this stage, it will be safe to say that ouabain inhibits the ATPase by binding to a cavity formed by the transmembrane helices M1, M2, M4, M5, and M6 near the K^+-binding sites with partial unwinding of the M4E helix. This unwinding might explain why ouabain binding is so slow (30).

Materials and Methods

Crystals of Na^+,K^+-ATPase from shark rectal gland were prepared in the E2·2K^+·MgF_4^{2-} form as described in ref. 16. After a dialysis against the crystallization buffer [25% glycerol (wt/vol), 5% (vol/vol) MPD, 100 mM potassium acetate, 10 mM KCl, 4 mM $MgCl_2$, 4 mM KF, 0.1 mM EGTA, 10 mM glutathione, 2 μg/mL 2,6-di-*t*-butyl-*p*-cresol, 20 mM Mes-Tris, pH 7.0] containing 40% (wt/vol) polyethylene glycol 3,000, the crystals were soaked in the same buffer but containing 20 mM ouabain for 5 h. They were flash-frozen in cold nitrogen gas. All of the diffraction data were collected at BL41XU of SPring-8 at 100 K using a Rayonix E255HE CCD detector. The wavelength used was 0.9 Å. Denzo and Scalepack (31) were used to process diffraction data, and the data from 2 best crystals were merged. An atomic model was built from the ouabain unbound form (PDB ID: 2ZXE) by molecular replacement and refined to R_{work} of 24.7% and R_{free} of 29.3% at 2.8 Å resolution with CNS (32) and Refmac (33). Fractions (%) of residues (altogether 1,134, excluding Gly and Pro) in the most favored/

additionally allowed/generously allowed/disallowed regions of Ramachandran plot are 84.8/15.1/0.1/0.0, respectively. Statistics for data collection and refinement are listed in Table 1. The model for the high affinity state was built according to the difference between the crystal structures of Ca^{2+}-ATPase in E2·MgF_4^{2-}(TG) (PDB ID: 1WPG) and E2·BeF_3^- (PDB ID: 2ZBE) (24) and energy minimized with CNS. Structural figures were prepared with TurboFRODO (http://www.afmb.univ-mrs.fr/-TURBO-) and PyMOL (http://www.pymol.org/).

ACKNOWLEDGMENTS. We thank Masahide Kawamoto and Nobutaka Shimizu (Japan Synchrotron Radiation Research Institute; JASRI) for their help in data collection at BL41XU, SPring-8, and Takeo Tsuda for many aspects of this work. We are grateful to David B. McIntosh and Steven Karlish for their help in improving the manuscript and Hanne R.Z. Christensen for her expert technical assistance. We also thank Franz Kerek for discussion. This work was supported by a Specially Promoted Project Grant from the Ministry of Education, Culture, Sports, Science, and Technology of Japan (C.T.) and grants from the Danish Medical Research Council (F.C.).

1. Prassas I, Diamandis EP (2008) Novel therapeutic applications of cardiac glycosides. *Nat Rev Drug Discov* 7:926–935.
2. Price EM, Rice DA, Lingrel JB (1990) Structure-function studies of Na,K-ATPase. Site-directed mutagenesis of the border residues from the H1–H2 extracellular domain of the α subunit. *J Biol Chem* 265:6638–6641.
3. Lingrel JB, Orlowski J, Price EM, Pathak BG (1991) Regulation of the α-subunit genes of the Na,K-ATPase and determinants of cardiac glycoside sensitivity. *Soc Gen Physiol Ser* 46:1–16.
4. Schultheis PJ, Wallick ET, Lingrel JB (1993) Kinetic analysis of ouabain binding to native and mutated forms of Na,K-ATPase and identification of a new region involved in cardiac glycoside interactions. *J Biol Chem* 268:22686–22694.
5. Feng J, Lingrel JB (1994) Analysis of amino acid residues in the H5–H6 transmembrane and extracellular domains of Na,K-ATPase alpha subunit identifies threonine 797 as a determinant of ouabain sensitivity. *Biochemistry* 33:4218–4224.
6. Palasis M, Kuntzweiler TA, Argüello JM, Lingrel JB (1996) Ouabain interactions with the H5–H6 hairpin of the Na,K-ATPase reveal a possible inhibition mechanism via the cation binding domain. *J Biol Chem* 271:14176–14182.
7. Crambert G, Schaer D, Roy S, Geering K (2004) New molecular determinants controlling the accessibility of ouabain to its binding site in human Na,K-ATPase α isoforms. *Mol Pharmacol* 65:335–341.
8. Qiu LY, Koenderink JB, Swarts HGP, Willems PHGM, De Pont JJHHM (2003) Phe783, Thr797, and Asp804 in transmembrane hairpin M5–M6 of Na^+,K^+-ATPase play a key role in ouabain binding. *J Biol Chem* 278:47240–47244.
9. Qiu LY, et al. (2005) Reconstruction of the complete ouabain-binding pocket of Na,K-ATPase in gastric H,K-ATPase by substitution of only seven amino acids. *J Biol Chem* 280:32349–32355.
10. Fullerton DS, Yoshioka K, Rohrer DC, From AH, Ahmed K (1980) A crystallographic, conformational energy, and biological study of Actodigin (AY-22,241) and its genin. *Mol Pharmacol* 17:43–51.
11. Yoda A (1974) Association and dissociation rate constants of the complexes between various cardiac monoglycosides and Na, K-ATPase. *Ann N Y Acad Sci* 242:598–616.
12. Paula S, Tabet MR, Ball WJ, Jr (2005) Interactions between cardiac glycosides and sodium/potassium-ATPase: Three-dimensional structure-activity relationship models for ligand binding to the E2-Pi form of the enzyme versus activity inhibition. *Biochemistry* 44:498–510.
13. Hansen O (1999) Heterogeneity of Na^+/K^+-ATPase from rectal gland of *Squalus acanthias* is not due to α isoform diversity. *Pflugers Arch* 437:517–522.
14. Forbush B, III (1983) Cardiotonic steroid binding to Na,K-ATPase. *Curr Topics Memb Transport* 19:167–201.
15. Or E, Goldshleger ED, Tal DM, Karlish SJ (1996) Solubilization of a complex of tryptic fragments of Na,K-ATPase containing occluded Rb ions and bound ouabain. *Biochemistry* 35:6853–6864.
16. Shinoda T, Ogawa H, Cornelius F, Toyoshima C (2009) Crystal structure of the sodium-potassium pump at 2.4 Å resolution. *Nature* 459:446–450.
17. Toyoshima C, Nomura H, Tsuda T (2004) Lumenal gating mechanism revealed in calcium pump crystal structures with phosphate analogues. *Nature* 432:361–368.
18. Glynn IM (1985) in *The Enzymes of Biological Membranes*, ed Martonosi AN (Plenum Press, New York, NY) 2nd Ed, Vol 3, pp 35–114.
19. Akera T, et al. (1985) Effects of K^+ on the interaction between cardiac glycosides and Na,K-ATPase. *Eur J Pharmacol* 111:147–157.
20. Rossi B, Ponzio G, Lazdunski M (1982) Identification of the segment of the catalytic subunit of Na^+,K^+ATPase containing the digitalis binding site. *EMBO J* 1:859–861.
21. Rathore H, From AH, Ahmed K, Fullerton DS (1986) Cardiac glycosides. 7. Sugar stereochemistry and cardiac glycoside activity. *J Med Chem* 29:1945–1952.
22. Arystarkhova E, Gasparian M, Modyanov NN, Sweadner KJ (1992) Na,K-ATPase extracellular surface probed with a monoclonal antibody that enhances ouabain binding. *J Biol Chem* 267:13694–13701.
23. Crambert G, et al. (2000) Transport and pharmacological properties of nine different human Na, K-ATPase isozymes. *J Biol Chem* 275:1976–1986.
24. Toyoshima C, Norimatsu Y, Iwasawa S, Tsuda T, Ogawa H (2007) How processing of aspartylphosphate is coupled to lumenal gating of the ion pathway in the calcium pump. *Proc Natl Acad Sci USA* 104:19831–19836.
25. Schönfeld W, et al. (1985) The lead structure in cardiac glycosides is 5 β, 14 β-androstane-3 β 14-diol. *Naunyn Schmiedebergs Arch Pharmacol* 329:414–426.
26. Sagara Y, Inesi G (1991) Inhibition of the sarcoplasmic reticulum Ca^{2+} transport ATPase by thapsigargin at subnanomolar concentrations. *J Biol Chem* 266:13503–13506.
27. Toyoshima C, Nomura H (2002) Structural changes in the calcium pump accompanying the dissociation of calcium. *Nature* 418:605–611.
28. Xu C, Ma H, Inesi G, Al-Shawi MK, Toyoshima C (2004) Specific structural requirements for the inhibitory effect of thapsigargin on the Ca^{2+} ATPase SERCA. *J Biol Chem* 279:17973–17979.
29. Tanenbaum DM, Wang Y, Williams SP, Sigler PB (1998) Crystallographic comparison of the estrogen and progesterone receptor's ligand binding domains. *Proc Natl Acad Sci USA* 95:5998–6003.
30. Wallick ET, Schwartz A (1988) Interaction of cardiac glycosides with Na^+,K^+-ATPase. *Methods Enzymol* 156:201–213.
31. Otwinowski Z, Minor W (1997) Processing of X-ray diffraction data collected in oscillation mode. *Methods Enzymol* 276:307–325.
32. Brünger AT, et al. (1998) Crystallography & NMR system: A new software suite for macromolecular structure determination. *Acta Crystallogr D* 54:905–921.
33. Murshudov GN, Vagin AA, Lebedev A, Wilson KS, Dodson EJ (1999) Efficient anisotropic refinement of macromolecular structures using FFT. *Acta Crystallogr D* 55:247–255.